Elucidating complex surface reconstructions with atomic-resolution scanning tunneling microscopy: Au(100)-aqueous electrochemical interface

Xiaoping Gao, Antoinette Hamelin,* and Michael J. Weaver
Department of Chemistry, Purdue University, West Lafayette, Indiana 47907
(Received 25 February 1992)

The utilization of scanning tunneling microscopy (STM) with high-quality atomic resolution for elucidating complex electrochemical surface reconstructions is illustrated for the Au(100)-aqueous interface. The reconstruction, triggered by negative surface electronic charges, exhibits typically a (5×27) symmetry involving quasihexagonal surface packing. The detailed atomic arrangements within the unit cell, including the spatial relationship of the reconstructed top layer to the underlying substrate, can be deduced from STM images featuring adjoining (5×27) and (1×1) domains. A number of subtly different superstructures could also be discerned; these are seen to arise from the need for the observed ribbonlike reconstructed domains to circumnavigate surface defects. The unique virtues of atomic-resolution STM for obtaining detailed local information on surface atomic arrangements in complex nonuniform systems are pointed out, along with its applicability (on an equal footing) to electrochemical as well as vacuum surface science.

The phenomenon of reconstruction at solid surfaces, whereby the top (and possibly also underlying) layers of atoms rearrange to form ordered structures that differ from a simple termination of the bulk-phase crystal, is extremely well known in surface science, particularly for metals.[1] To date, most metal reconstructions have been studied by means of diffraction techniques, especially low-energy electron diffraction (LEED), in ultrahigh-vacuum (UHV) environments. Although powerful, these methods can face difficulties in analyzing reconstructions involving complex unit cells or the mixture of structures which often are anticipated to be present, especially on imperfectly ordered samples.

The emergence of scanning tunneling microscopy (STM) as a viable atomic-resolution structural probe[2] is providing intriguing opportunities for exploring surface reconstruction, as well as the real-space arrangements of atomic and molecular adlayers. Unlike diffraction methods, which reflect the reciprocal-space lattice periodicity over long distances, STM is an inherently local structural technique. While this latter property has been viewed as a limitation of STM, it can nonetheless offer unique opportunities for the exploration of real-space atomic distributions over a spectrum of distance scales. The technique should therefore be capable of elucidating individual components of complex surface structures, providing that true atomic resolution (i.e., observation of individual surface atoms) can be achieved.

Such individual atom-resolution STM images have recently been shown to be obtainable at monocrystalline metal-solution (i.e., electrochemical) interfaces[3-8] as well as in air and in UHV. Besides their practical importance, the *in situ* electrochemical systems enable both physical[3-7] and chemical[8] surface transformations, induced by alterations in the electrode potential, to be explored by STM. We have demonstrated recently that unusually high-quality STM data of this type can be obtained at ordered gold-aqueous interfaces.[5-7] Reconstruction is seen to be triggered on all three low-index gold surfaces by altering the potential to values corresponding to small ($10-15$ $\mu C\,cm^{-2}$) negative surface electronic charges.[5-7] The Au(100) surface is especially interesting in that the unreconstructed square-planar lattice is transformed into an undulating quasihexagonal atomic arrangement.[5] While the broad features of this reconstruction have succumbed to repeated scrutiny by diffraction and related methods over the last ten years, (for example, see Refs. 9–13), the detailed nature of the superlattice remains distinctly unclear. This situation reflects both the presence of a large unit cell [described variously as $(5\times20),c(26\times68)$, etc.] together with the likelihood of uniform structures.

We report here detailed atomic-resolution STM images obtained for ordered Au(100) in aqueous 0.1 *M* $HClO_4$ under electrode-potential control which enable the complexities and nuances of the reconstruction to be assessed anew. Besides providing the first comprehensive picture of reconstruction at an *in situ* electrochemical interface, the findings illustrate in a more general vein the power of STM for elucidating previously unobtainable details of surface atomic structures. Such local structural information can contribute importantly to a deeper understanding of atomic-level surface organization.

EXPERIMENTAL SECTION

The experimental STM procedures are largely as described elsewhere.[5-7,14] The microscope is a Nanoscope II (Digital Instruments) with a bipotentiostat for electrochemical STM. The STM tips were 0.01 in. tungsten wire etched electrochemically in 1 *M* KOH. Most STM images were obtained in the so-called "height mode" (i.e., at constant current). The set-point current was typically 10–20 nA, and the bias voltage ±10 mV. The faradaic leakage current was usually much smaller, ≤0.1 nA. The Au(100) crystal (hemisphere, 5 mm diameter) was

prepared at LEI-CNRS (see Appendix of Ref. 15). It was flame annealed, cooled in ultrapure water, and transferred to the STM cell, containing 0.1 *M* $HClO_4$, protected by a drop of water. The cell was refilled two to three times with fresh 0.1 *M* $HClO_4$ after assembly. The STM electrochemical cell wall, machined from Teflon, is secured to the base by a pair of set screws. The substrate surface formed the base of this cell. The cell holder, machined from Kel-F, contains the counter and reference electrode connections. The former was platinum and the latter was a freshly electro-oxidized gold wire. All electrode potentials quoted here, however, are converted to the saturated calomel electrode (SCE) scale.

RESULTS AND DISCUSSION

Following the flame annealing-water cooling pretreatment procedure, as discerned from STM the Au(100) surface is initially largely unreconstructed if the potential is held above approximately 0 V vs SCE.[5,16] An example of such an unfiltered STM image is shown in Fig. 1; the square array of spots (i.e., tunneling maxima) spaced 2.9($\pm$0.2) Å apart as expected for the (1×1) structure, is clearly evident. As noted in Ref. 5, however, altering the potential to lower values yielded dramatic changes in the surface structure within a few minutes. A good example of the progression of this reconstruction is shown as a mildly filtered height-shaded image in Fig. 2, obtained 10 min after stepping the potential to −0.3 V. While the center right-hand portion of the image shows the (1×1) atomic arrangement, a markedly corrugated structure is evident throughout the left-hand region. Close inspection of the latter reveals several features of interest. While the darkest (i.e., deepest) rows of gold atoms along each furrow are not easily discerned throughout Fig. 2, six gold atoms are seen to be packed across each strand in the same space as occupied by five atoms in the (1×1) structure. The consequent 20% higher atomic density across the furrows yields a quasihexagonal packing in place of the square-planar array for the unreconstructed surface.

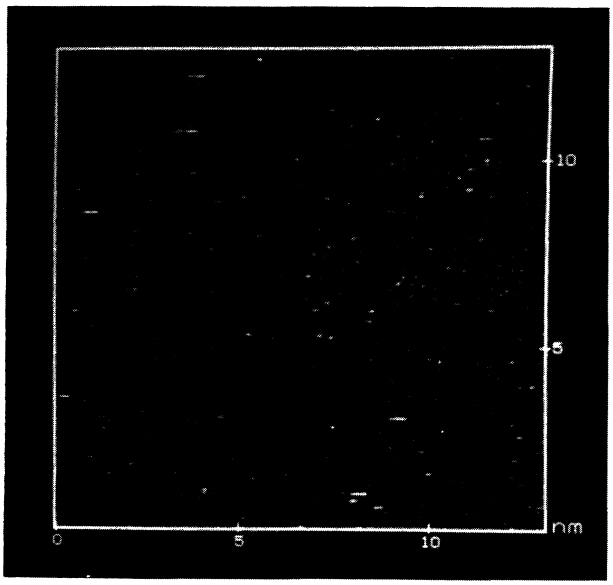

FIG. 1. Unfiltered top view atomic-resolution STM image of unreconstructed Au(100) in aqueous 0.1 *M* $HClO_4$ at −0.1 V vs SCE.

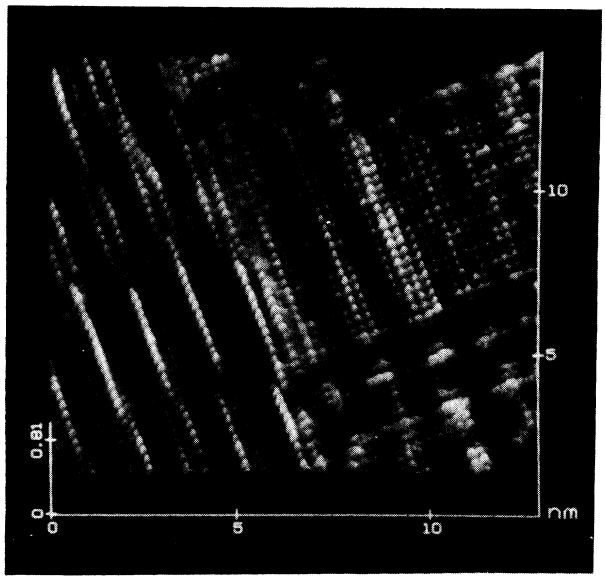

FIG. 2. Height-shaded atomic-resolution STM image at −0.3 V vs SCE, showing emergence of (5×27) reconstruction and adjoining (1×1) domain.

While the time taken for the reconstruction to develop depended somewhat on the applied potential, the formation of the corrugated structure was generally complete within 20–30 min, and stable thereafter. The formation of the reconstruction was unaffected by the presence of the tip, as deduced by altering the scanning area during a temporal measurement sequence. This situation differs markedly from measurements on Au(111) in air using much higher (about 1 V) bias voltages, where reconstruction is seen to be triggered by the local fields surrounding the tip.[17] The relatively low gap resistances employed in the present work enabled the atomic corrugations within the reconstructed as well as (1×1) domains to be clearly observed. For markedly higher gap resistance, however, atomic resolution was readily discernible only within the latter domains.

A more subtle, yet striking, structural pattern is also evident along the reconstructed rows in Fig. 2. Single-strand segments of bright (i.e., highest) atoms are seen, spaced 14.5 ($\pm$0.5) Å apart, which are interspersed periodically by "dual-atom" sectors. The length of both these single- and double-strand segments is usually 14 atoms (but sometimes 13 or 15). A comparable symmetry pattern, yet without atomic resolution, was also discussed in an early STM study for Au(100) in UHV.[18] In our preliminary report, we attributed distinct structures (labeled I and II) to the single- and double-strand segments.[5] It is now apparent that this periodic alteration together constitutes a single superstructure, having usually a (5×27) unit cell.

Two pieces of information obtainable from images such

as Fig. 2, featuring adjoining reconstructed and (1×1) domains, allow a confident assignment of the detailed unit-cell structure. First, the atom spacing along the rows is slightly, yet significantly, compressed compared with that in the (1×1) lattice. By inspecting (1×1) rows paralleling nearby reconstructed regions, the 14 atoms in the latter strand segments are seen to have the same length, 39 Å, as that occupied by 13.5 gold atoms in the (1×1) lattice. This 3.6% atomic compression is in harmony with recent high-resolution LEED data.[12] [Note that the tactic of comparing lattice spacings along neighboring domains enables the interatomic spacings of the reconstruction with respect to the (1×1) substrate to be determined with excellent precision.]

Second, the registry between the reconstructed top atomic layer and the underlying substrate can be deduced from the adjoining-domain images by extrapolating the observed crosswise (1×1) row directions into a reconstructed surface region. This tactic enables one, for instance, to infer that the center atom in each 14-atom single strand is situated directly atop an underlying substrate atom (assuming the latter to be unreconstructed). Given the observed compression along the strands, the atoms therefore occupy "coordination sites" that undergo a periodic transition from atop to twofold bridge every 14 atoms. This deduction is consistent with the maximum "brightness" (i.e., highest Z displacement) observed in the middle of the single-strand segments (Fig. 2), the atoms of which occupy atop sites. Taken together, these two pieces of information also suggest that the immediately underlying substrate lattice indeed forms the anticipated (1×1) structure; i.e., that reconstruction is limited largely to the top layer of atoms.

A ball model of the inferred top-layer structure (grey shaded) with respect to the underlying substrate lattice is shown in Fig. 3. For simplicity, this figure depicts half of the inferred (5×27) unit cell, the remainder (above or below) being simply the mirror image. A similar, (5×28), unit cell was deduced recently for Au(100) in UHV by means of high-resolution LEED.[12] It is worth emphasizing further the value of atomic-resolution STM images for resolving such precise structures. The uncertainty in the piezoelectric calibration (say, ±10%) limits inevitably the evaluation of absolute atomic-scale distances by STM. However, the diverse supplementary information contained in atomic-resolution images, such as corrugation periodicities and the registry between adjoining reconstructed and (1×1) domains as utilized here, can enable much more precise (and detailed) spatial information to be extracted than might be expected at first sight.

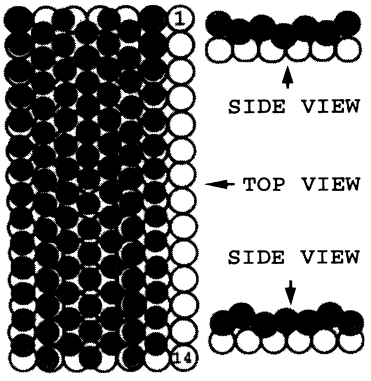

FIG. 3. Ball model depicting half a unit cell of proposed (5×27) reconstruction.

While propagation of the usual (5×27) superstructure is reproducibly observed in the STM images, especially within large domains, several closely related, yet distinct, structures are also prevalent in local patches across the surface. Figures 4(a)–4(d) show height-shaded STM images of the most recurrent structural patterns. Most of Fig. 4(a) and part of Fig. 4(b) display the same undulating pattern ("single-to-double strand") as in Fig. 2. Some asymmetry is seen, however; thus the far left-hand row in Fig. 4(b) exhibits instead a "single-to-single" pattern. The structural transition from a double to single row pattern seen from right to left in the top (but not the bottom) half of Fig. 4(b) is consistent with the large unit-cell dimension (either 48 or 68) deduced from LEED.[9,12] Comparison of the STM images with the ball model (Fig. 3) indicates that the overlayer is contracted by approximately 0.8% across the rows, so that the (5×27) unit cell is slightly incommensurate with the underlying lattice (cf. Ref. 18). Interesting details of the transition between the (1×1) and reconstructed domains are evident towards the right-hand edge of Fig. 4(b). More marked asymmetries are seen in Figs. 4(c) and 4(d). In the former, a propagation of largely "single-strand" rows is seen, being interrupted by a one-atom lateral shift in the middle of the image. Figure 4(d) shows a comparable one-atom jog, but with the rows having a predominantly "double-strand" character.

These structural mutations can be described readily by minor modifications in the model given in Fig. 3, which involve making the top-layer atom strings slightly nonparallel to the underlying substrate rows. For example, if the top-layer atoms in the horizontal line marked "1" in Fig. 3 are shifted to the left by approximately 0.5 Å they present an arrangement which is identical to that for the bottom (double-strand) line, marked 14, except that the former has a periodicity which is shifted laterally by one atomic spacing. This structural modification can be achieved merely by rotating the top-layer lattice counterclockwise by 0.7° with respect to the underlying substrate. The corrugated appearance of Fig. 4(d) is nicely consistent with such a structure. Similarly, shifting the top-layer atoms in line 14 by 0.5 Å to the left yields a single-strand symmetry as seen in line 1. Clockwise rotation of the top-layer lattice by 0.7° yields a row periodicity that matches the structure seen in Fig. 4(c).

The appearance of such distinct superstructures raises the question of the reason for their existence. At least a partial answer can be obtained by inspecting a variety of STM images obtained for larger surface areas. Illustrative examples are shown in Figs. 5(a)–5(d). Present in the former image are two "mesas," i.e., small flat regions raised by a monatomic step above the surrounding (100)

domain. [These appear as bright regions in the bottom left-hand and middle right-hand regions of Fig. 5(a).] The influence of the latter mesa upon the nearby reconstruction is readily apparent. The atomic strands, starting in the bottom right-hand corner of the image, are seen to "sidestep" this defect by making repeated jogs towards the left. These mesas are seen to be present prior to the initiation of the reconstruction process.

Consequently, then, the nominally linear (5×27) reconstruction is able to circumnavigate surface defects. An interesting limitation to the flexibility of such strand propagation, however, is evident in that the region immediately above and below the right-hand mesa in Fig. 5(a) is seen to remain unreconstructed. These points are further evident in the large-area images shown in Figs. 5(b)–5(d). A number of mesas are seen in these images, which clearly affect the propagation and direction of the reconstruction strands. [The mesas may well be produced from the excess gold atoms freed by lifting the Au(100) surface reconstruction during the water-cooling step after flame annealing.] Several other significant structural features can be gleaned from such large-area images. While the reconstruction is seen to proceed along both possible orientations (90° to each other) on the square-planar substrate, it occurs preferentially along directions where lengthy ($\gtrsim 300$ Å) strands can be pro-

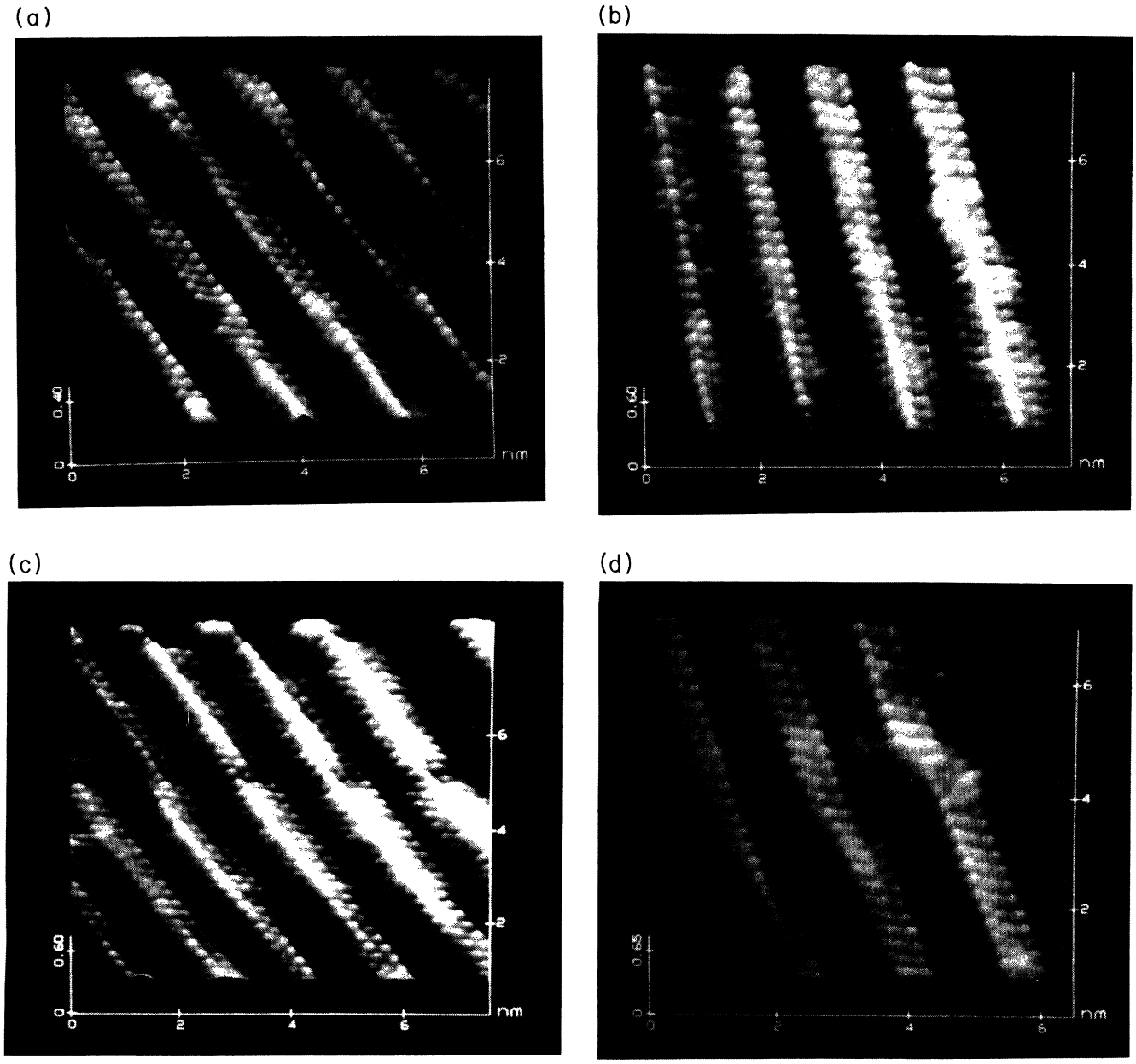

FIG. 4. Height-shaded atomic-resolution STM images at −0.3 V vs SCE showing various common reconstruction superstructures.

duced. The corrugated rows therefore often lie parallel to terrace edges, as seen in Fig. 5(d). This tendency presumably reflects an energy cost of terminating the chains. Nevertheless, separate 90° rotated strand domains are often seen to "cross" each other, as evident in Fig. 5(b). In most cases, one of the two 90° strand domains is seen to be terminated at the crossing point. Occasionally [as seen in Fig. 5(c)], corrugated rows are also seen to propagate over small mesas. Temporal sequences of such images obtained after initiating the reconstruction can also yield information on the formation mechanisms; these show that the 24% additional gold atoms necessary to form the (5×27) single lattice diffuse from terrace edges and other surface defects, especially small mesas.[19]

The domain lengths in a direction normal to the corrugated strands are often limited to $\lesssim 5$ unit cells. Even single reconstructed strands were occasionally observed, consisting of quasihexagonal ribbons, three atoms wide. An example is shown in Fig. 6(a). In this case, a pair of parallel ribbons, about 60 Å apart, are observed to lie on the (1×1) substrate. Unlike the usual quasihexagonal reconstruction described above, the gold interatomic spacing along the row direction is commensurate with the substrate lattice (i.e., is not compressed significantly). Over a 5-min period, these individual strands were ob-

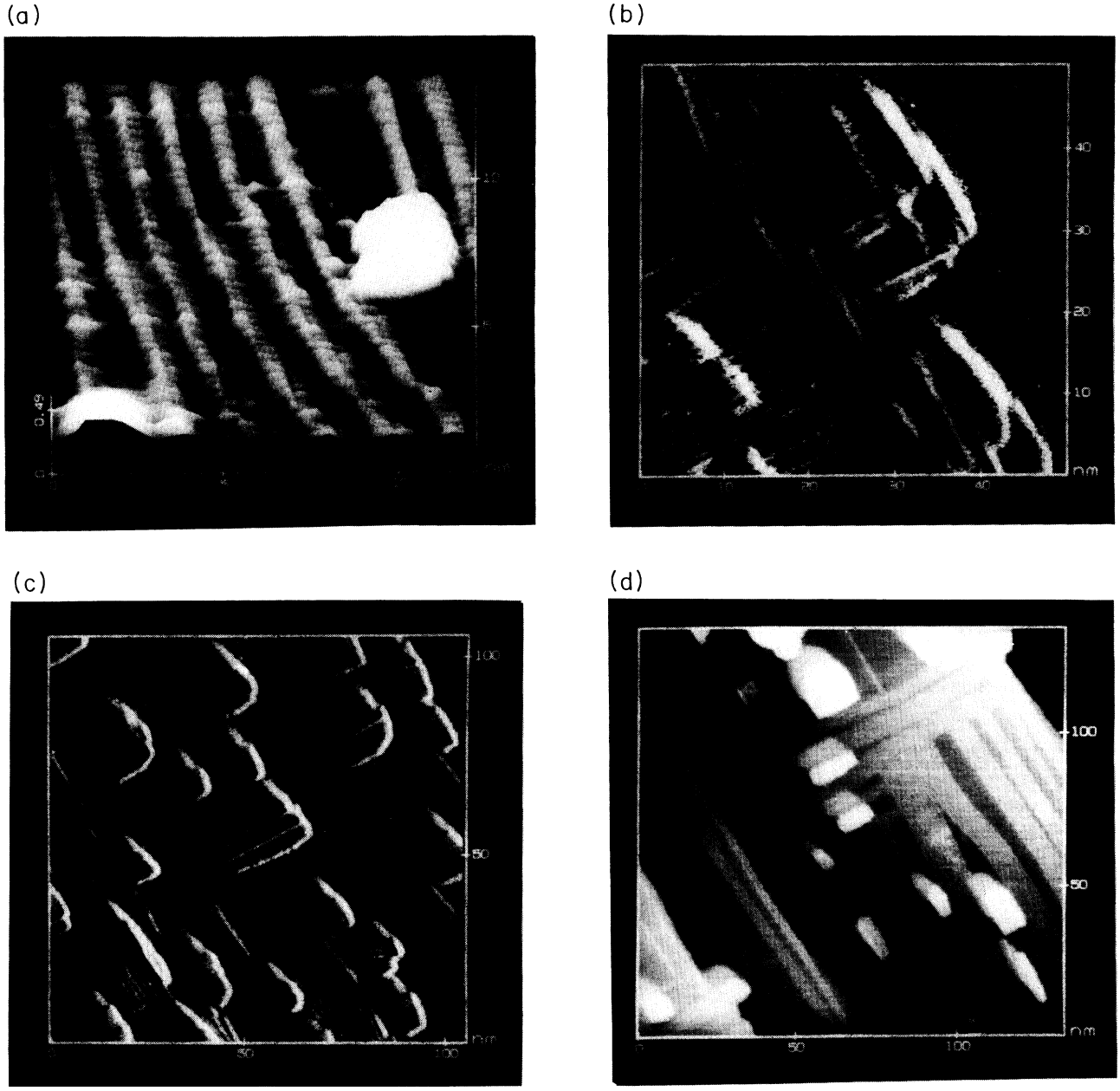

FIG. 5. Larger-area STM images of Au(100) reconstruction at -0.3 V vs SCE, showing long-range structural propagations, and the effect of mesas.

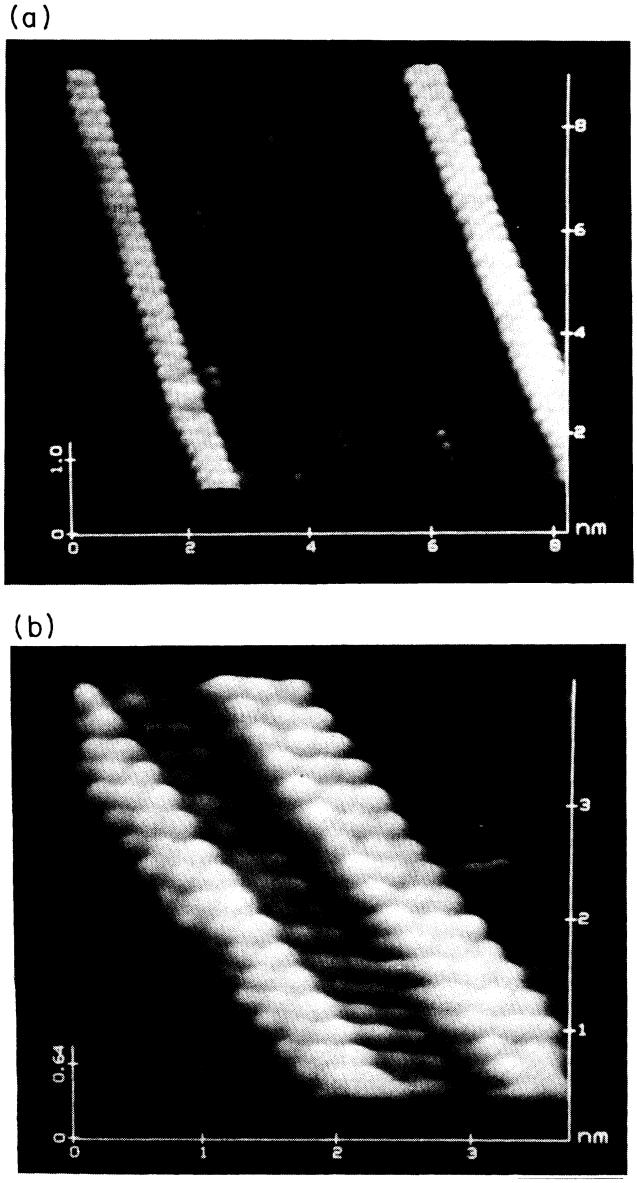

FIG. 6. Height-shaded images of single-strand reconstruction pattern on the (1×1) substrate, obtained at -0.2 V vs SCE.

served to diffuse together to form the coalesced domain depicted in Fig. 6(b).

Generally, raising the potential above 0.2 V resulted in a gradual lifting of the reconstruction, predominantly (1×1) domains returning over approximately a 10-min period.[5] Detailed examination of this phenomenon, however, was hampered by instability of the tungsten tip at such positive potentials. Nevertheless, preliminary data obtained for Au(100) in iodide-containing solutions show the potential-induced formation and lifting of the (5×27) reconstruction to be largely reversible, and also remarkably rapid ($\lesssim 1$ s). The effect of anion adsorption on Au(100) reconstruction is currently undergoing detailed examination in our laboratory.

Overall, the present results illustrate in general terms some of the avenues, so far largely unexplored, by which STM can be utilized to unravel details of metal surface structure when such high-quality atomic-resolution images can be obtained. The inherently "local" nature of the STM probe clearly enables individual, subtly different, structural components to be separately identified, and their role in the superlattice propagation assessed. Such information is difficult to obtain from diffraction or other "averaging" techniques. Insight can also be obtained from STM into several related matters, including the atomic arrangements at domain boundaries and the dynamics and likely mechanisms of reconstruction.

Perhaps most importantly, these fundamental issues can now be addressed for *in situ* electrochemical interfaces under potential control in a similar fashion as for the metal-UHV systems so far prevalent in surface science. The ability to trigger surface structural transformations by means of this external electrical variable brings additional significance to the former systems. Furthermore, electrochemical interfaces offer an environment especially conducive to STM experiments, in that the surface can be maintained in a relatively clean and well-defined state while enabling tips to be loaded and replaced much more readily than in UHV systems. The relative paucity of atomic-resolution STM data for metal-UHV systems of the quality described here and elsewhere for electrochemical interfaces most likely reflects these factors. The recent demonstration, specifically for Au(100), that x-ray-diffraction techniques can also be harnessed to yield detailed atomic structural information in electrochemical environments[13(b),20] is also very promising, especially given its complementary nature to STM. There is ample evidence, then, to expect both these methods to contribute centrally to the development of an era of atomic-level understanding in electrochemical surface science.

ACKNOWLEDGMENTS

This work was supported by the Office of Naval Research and the National Science Foundation.

*Permanent address: Laboratoire d'Electrochimie Interfaciale du CNRS, 1 place A. Briand, 92195 Meudon, France.

[1]See, for example, M. A. Van Hove, S.-W. Wang, D. F. Ogletree, and G. A. Somorjai, Adv. Quantum Chem. **20**, 1 (1989); S. Pick, Surf. Sci. Rep. **12**, 99 (1990).

[2]For a recent review, see F. Ogletree and M. Salmeron, Prog. Solid State Chem. **20**, 235 (1990).

[3]O. M. Magnussen, J. Hotlos, R. J. Nichols, D. M. Kolb, and R. J. Behm, Phys. Rev. Lett. **64**, 2929 (1990).

[4]S.-L. Yau, X. Gao, S.-C. Chang, B. C. Schardt, and M. J. Weaver, J. Am. Chem. Soc. **113**, 6049 (1991).

[5]X. Gao, A. Hamelin, and M. J. Weaver, Phys. Rev. Lett. **67**, 618 (1991).

[6]X. Gao, A. Hamelin, and M. J. Weaver, J. Chem. Phys. **95**, 6993 (1991).

[7]X. Gao, A. Hamelin, and M. J. Weaver, Phys. Rev. B **44**,

10 983 (1991).
[8]X. Gao, Y. Zhang, and M. J. Weaver, J. Phys. Chem. **96**, 4156 (1992).
[9]M. A. Van Hove, R. J. Koestner, P. C. Stair, J. P. Biberian, L. L. Kesmodel, I. Bartos, and G. A. Somorjai, Surf. Sci. **103**, 189 (1981).
[10]K. H. Rieder, T. Engel, R. H. Swendsen, and M. Manninen, Surf. Sci. **127**, 223 (1983).
[11]K. Yamazaki, K. Takayanagi, Y. Tanishiro, and K. Yagi, Surf. Sci. **199**, 595 (1988).
[12]Y.-F. Liew and G.-C. Wang, Surf. Sci. **227**, 190 (1990).
[13](a) S. G. J. Mochrie, D. M. Zehner, B. M. Ocko, and D. Gibbs, Phys. Rev. Lett. **64**, 2925 (1990); (b) B. M. Ocko, J. Wang, A. Davenport, and H. Isaacs, *ibid.* **65**, 1466 (1990).
[14]C. Vitus, S.-C. Chang, B. C. Schardt, and M. J. Weaver, J. Phys. Chem. **95**, 7559 (1991).
[15]A. Hamelin, S. Morin, J. Richer, and J. Lipkowski, J. Electroanal. Chem. **285**, 249 (1990).
[16]A. Hamelin, X. Gao, and M. J. Weaver, J. Electroanal. Chem. **323**, 361 (1992).
[17]J. M. Schott and H. S. White, Langmuir (to be published).
[18]G. K. Binnig, H. Rohrer, Ch. Gerber, and E. Stoll, Surf. Sci. **144**, 321 (1984).
[19]X. Gao, A. Hamelin, and M. J. Weaver (unpublished).
[20]B. Ocko *et al.* (unpublished).

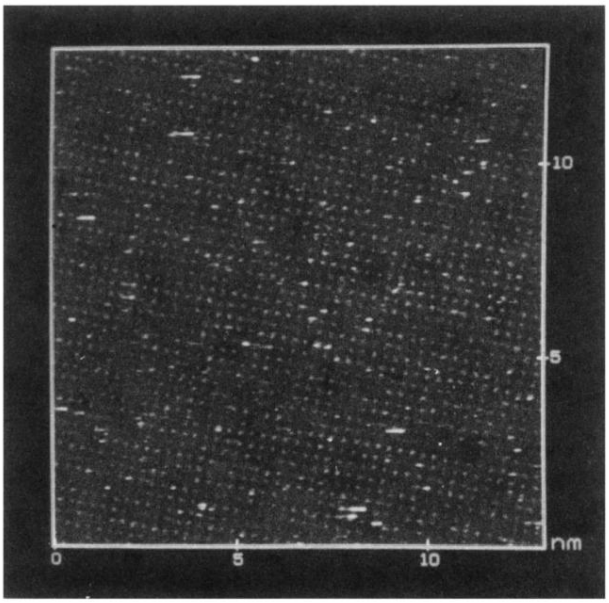

FIG. 1. Unfiltered top view atomic-resolution STM image of unreconstructed Au(100) in aqueous 0.1 *M* $HClO_4$ at −0.1 V vs SCE.

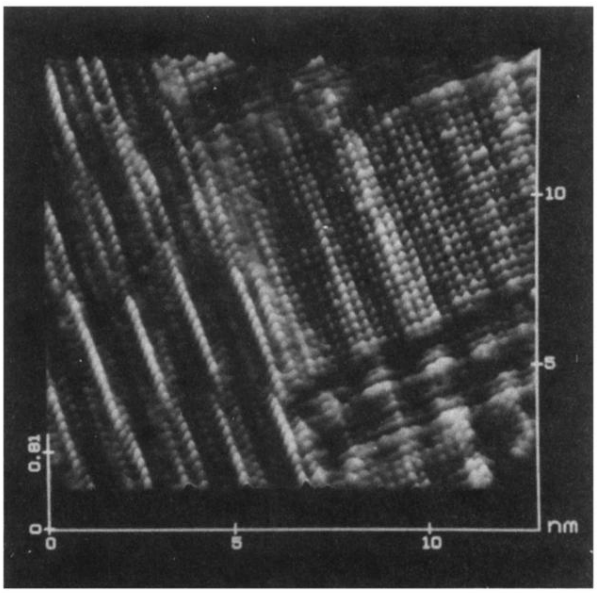

FIG. 2. Height-shaded atomic-resolution STM image at −0.3 V vs SCE, showing emergence of (5×27) reconstruction and adjoining (1×1) domain.

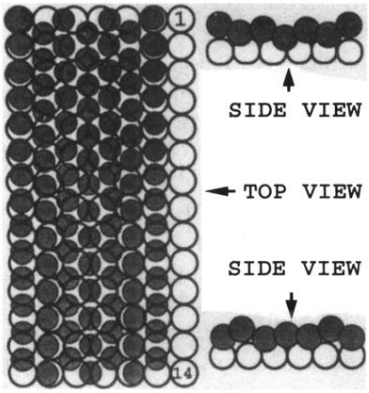

FIG. 3. Ball model depicting half a unit cell of proposed (5×27) reconstruction.

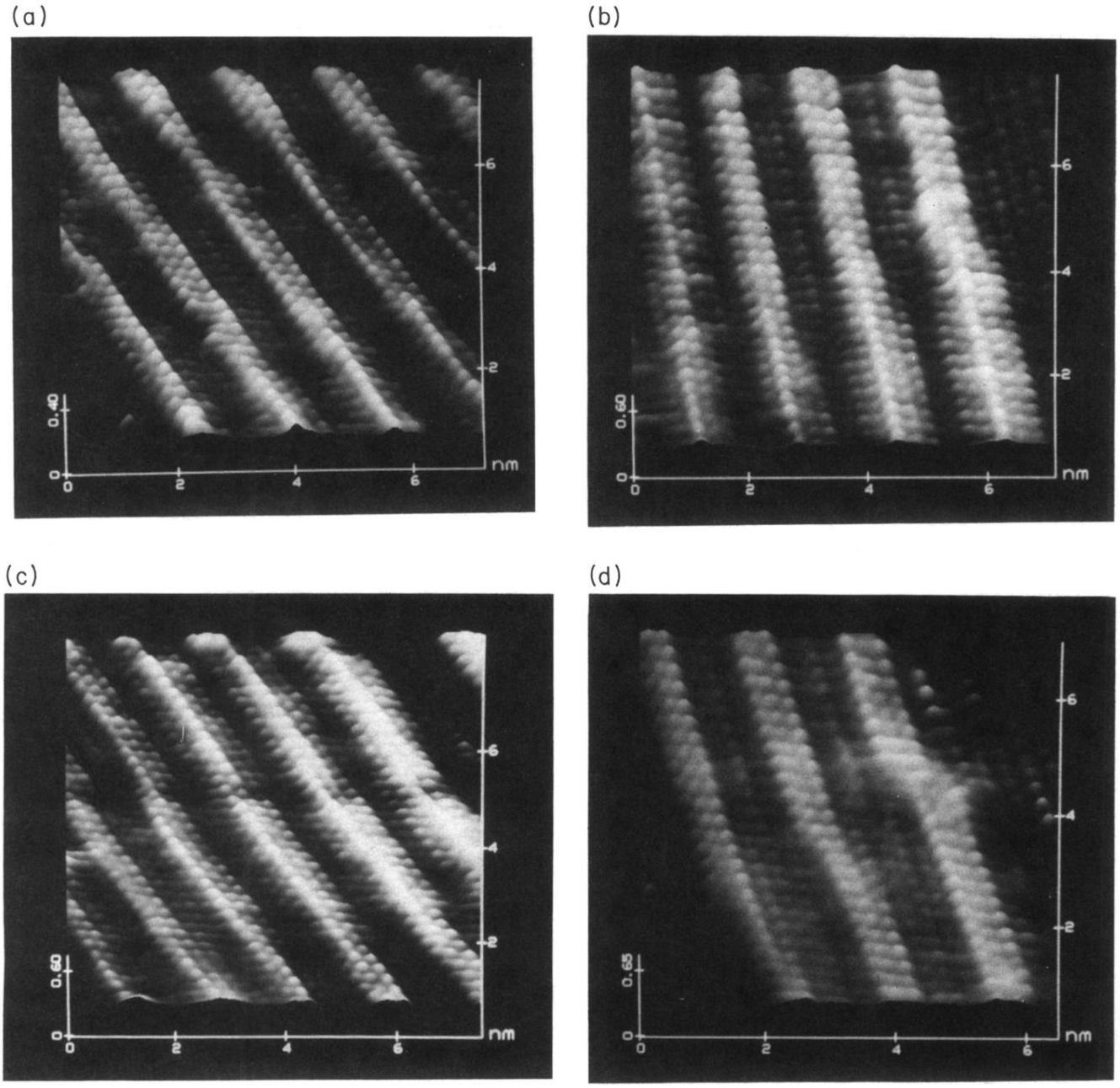

FIG. 4. Height-shaded atomic-resolution STM images at −0.3 V vs SCE showing various common reconstruction superstructures.

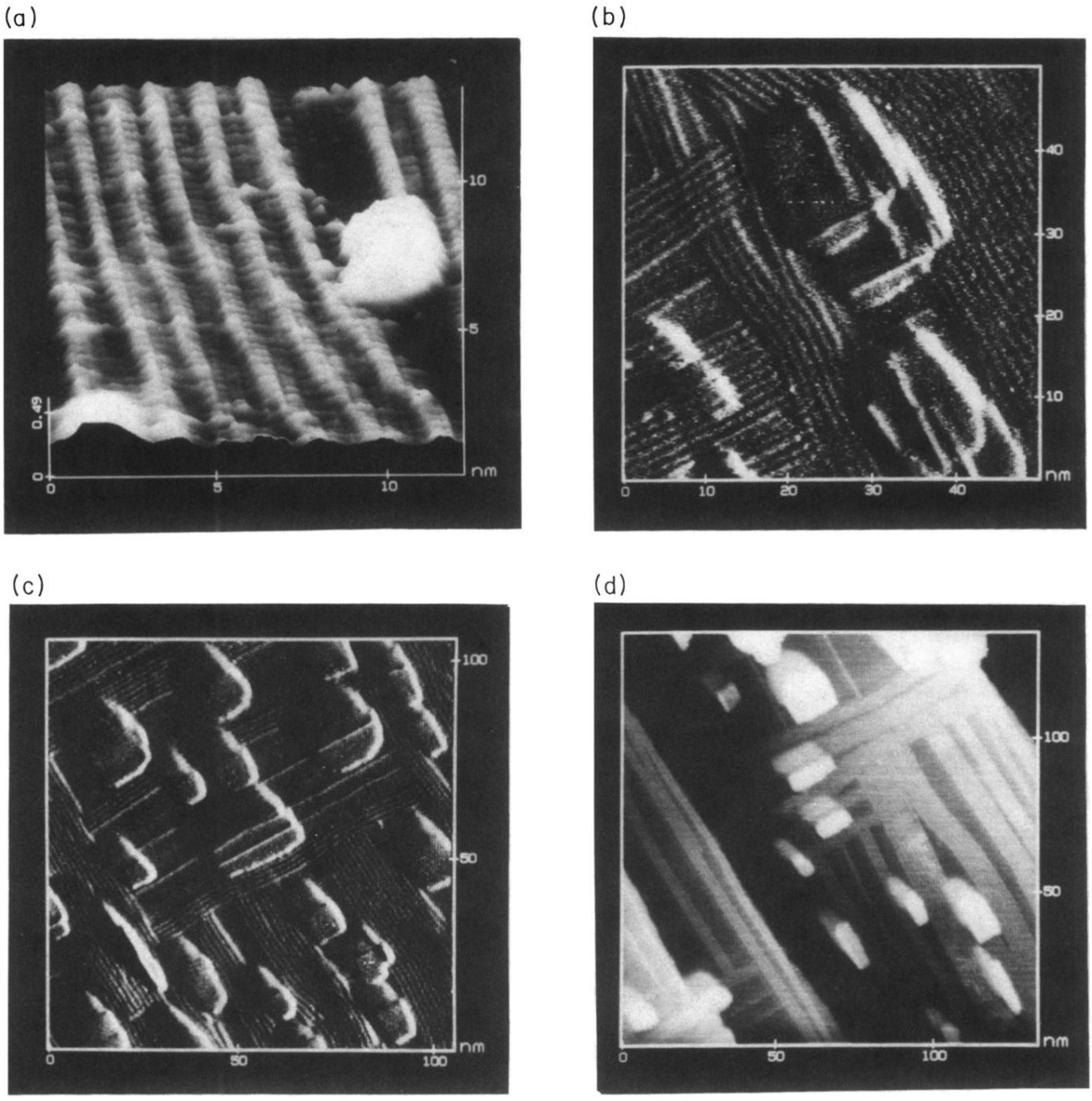

FIG. 5. Larger-area STM images of Au(100) reconstruction at −0.3 V vs SCE, showing long-range structural propagations, and the effect of mesas.

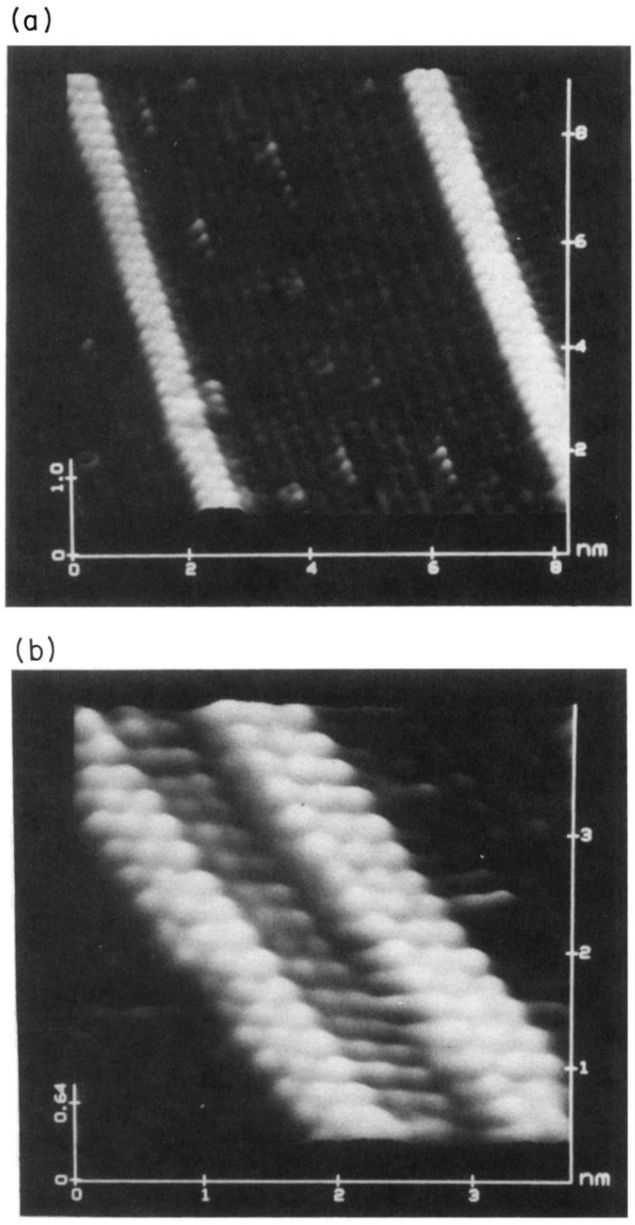

FIG. 6. Height-shaded images of single-strand reconstruction pattern on the (1×1) substrate, obtained at -0.2 V vs SCE.